

Supporting Information for:
Ordered Superstructures of a Molecular Electron
Donor on Au(111)

A. Mehler,^{†,¶} T. Kirchhübel,^{‡,¶} N. Néel,[†] F. Sojka,[‡] R. Forker,[‡] T. Fritz,[‡] and J.
Kröger^{*,†}

*Institut für Physik, Technische Universität Ilmenau, D-98693 Ilmenau, Germany, and
Institut für Festkörperphysik, Friedrich-Schiller-Universität Jena, D-07743 Jena, Germany*

E-mail: joerg.kroeger@tu-ilmenau.de

*To whom correspondence should be addressed

[†]Institut für Physik, Technische Universität Ilmenau, D-98693 Ilmenau, Germany

[‡]Institut für Festkörperphysik, Friedrich-Schiller-Universität Jena, D-07743 Jena, Germany

[¶]These authors contributed equally to this work.

Au(111) Step Edges: Decoration by Single Molecules and Influence on *A*- and *B*-Phase Domains

STM images of a submonolayer DBP on Au(111) are shown in Figure S1. The Au(111) step edges are decorated prior to the formation of larger *A*-phase domains on the terraces. The majority of DBP molecules adsorb with their long molecular axes nearly perpendicular to the step edges. A few DBP molecules adsorb with their long molecular axes parallel to the step edges. The hcp stacking regions between two dislocation lines of the Au(111) reconstruction act as preferred adsorption sites for these molecules.

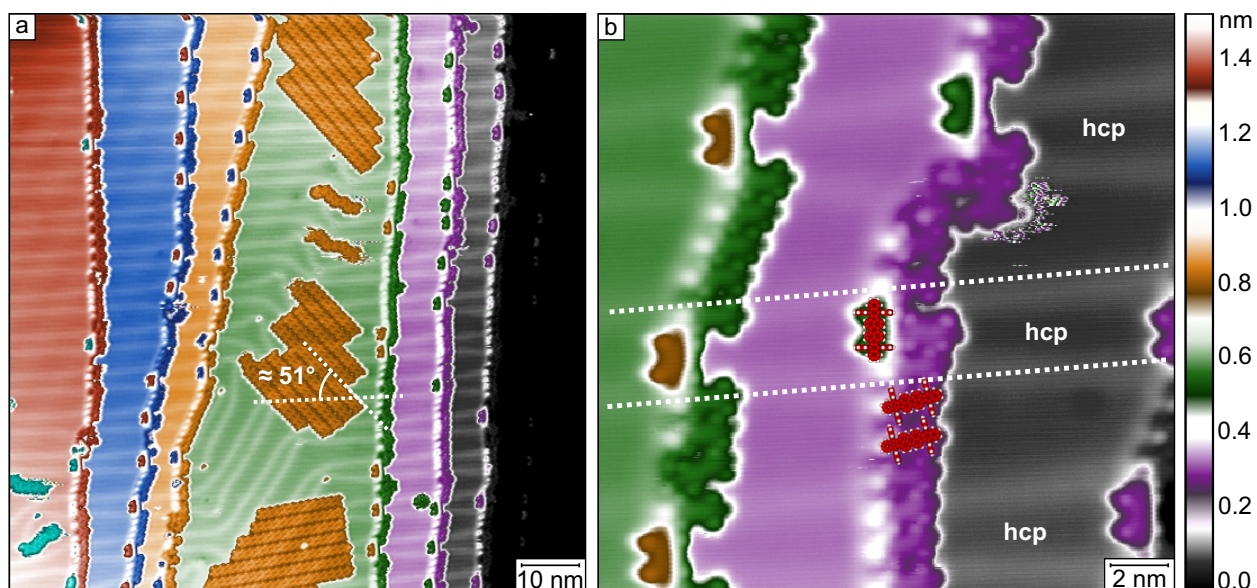


Figure S1: (a) Overview STM image of Au(111) covered with 0.4 MLE of DBP. The substrate step edges are decorated by DBP molecules (1.2 V, 50 pA, 100 nm \times 100 nm). Predominantly on top of the Au(111) hcp stacking regions, some of these molecules adopt parallel alignments to the step edges. Islands of DBP molecules assembled in the *A*-phase are visible on the central Au(111) terrace. For each domain, the short adsorbate unit cell vector encloses an angle of $\approx 51^\circ$ with the direction of the dislocation lines underneath. (b) Close-up STM image showing the decoration of step edges by DBP molecules, whose orientation depends on the Au(111) stacking region underneath (1 V, 50 pA, 20 nm \times 20 nm). In both images the majority of molecules bridges neighboring terraces in a perpendicular alignment.

Figure S2 shows representative STM images of Au(111) covered with *A*-phase and *B*-phase DBP domains. From the overview topographic data (Figure S2a) one may infer

that *A*-phase domains do not touch Au(111) step edges while *B*-phase domains do. This impression is corroborated by the close-up STM images in Figure S2b, c. *A*-phase islands tend to avoid contact with substrate step edges. In contrast, *B*-phase islands are attached to ascending as well as to descending step edges.

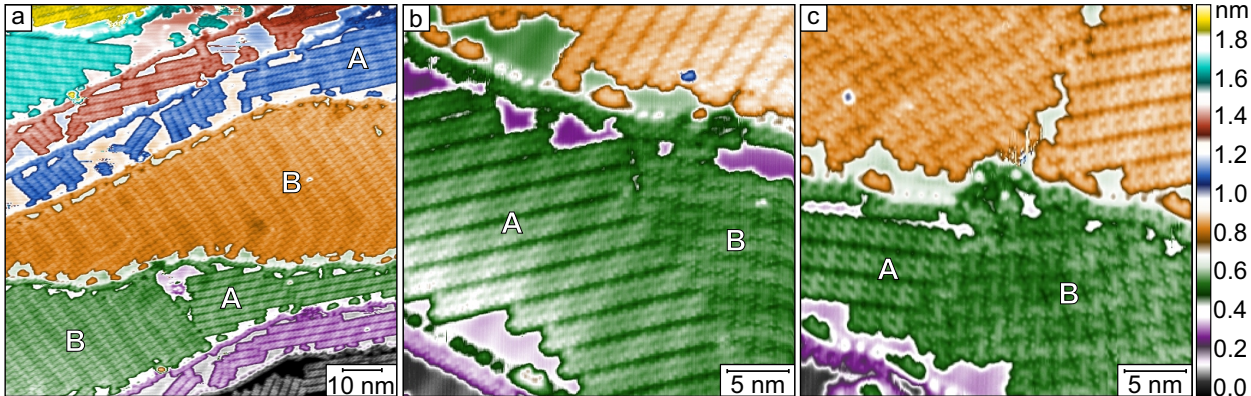


Figure S2: (a) Overview STM image of Au(111) covered with *A*-phase and *B*-phase DBP molecules (1 V, 50 pA, 96 nm \times 96 nm). (b), (c) Close-up STM images showing *A*-phase and *B*-phase domains close to Au(111) step edges (1 V, 50 pA, 32 nm \times 32 nm).

Interaction between the DBP Adsorption Phases and the Au(111) Surface Reconstruction

A Phase

The *A*-phase domains of DBP on Au(111) exhibit a high lateral order and their orientations are mainly determined by the Au(111) surface reconstruction underneath. Frequently, the short lattice vector of the *A* unit cell encloses an angle of $\approx 39.2^\circ$ with the reconstructed Au(111) direction, $\langle 1\bar{1}0 \rangle$, corresponding to $\approx 50.8^\circ$ with the Au(111) dislocation lines, which are aligned along $\langle 11\bar{2} \rangle$. These angles are derived from the analysis of multiple STM images and the results of LEED experiments, which are summarized in Table 1 of the main text. The preferred orientations are also adopted by the small *A*-phase domains in the STM image of Figure S1a. The molecular lattice usually remains unchanged when the Au(111)

reconstruction underneath changes its direction.

The influence of the A -phase domains on the Au(111) surface reconstruction is less obvious at first glance. In the following we analyze the periodicity of the surface reconstruction underneath the A -phase domain, which is shown in Figure S3. To this end, the epitaxy matrix of phase A with respect to the $(22 \times \sqrt{3})$ reconstruction is calculated by multiplication of the matrix from Table 1 with the epitaxy matrix of the $(22 \times \sqrt{3})$ supercell. Inversion results in the matrix $\mathbf{S} = \begin{pmatrix} 4.18 & 1.91 \\ 0.24 & 0.18 \end{pmatrix}$, which describes the relationship between the undistorted $(22 \times \sqrt{3})$ reconstruction and the A -phase lattice.

The periodicities of the molecular lattice as well as the Au(111) dislocation lines are clearly visible in the STM image in Figure S3a and, thus, the corresponding frequencies appear as spots in the fast Fourier transform (FFT) (Figure S3b). As the FFT of STM images can be treated similarly to LEED images,³ the software LEEDLab was used for the analysis.² The green dots of the simulated diffraction pattern in Figure S3b–d were fit to the most intense spots of the FFT, which originate from the A -phase lattice. This determines the sheared A -phase lattice in reciprocal space and in real space as well. Applying the epitaxy matrix \mathbf{S} to the real-space A -phase lattice, one obtains the direction of the sheared $(22 \times \sqrt{3})$ reconstruction, as expected from LEED measurements.

Centered around the intense adsorbate spots in the FFT, parallel rows of faintly visible spots provide information about the periodicity of the Au(111) surface reconstruction observed with STM. These spots originate from a convolution of the adsorbate lattice and the dislocation line periodicity. An analogue in LEED experiments is the multiscattering of electrons at the adsorbate and the substrate lattice. Thus, one can use the multiscattering feature of LEEDLab in order to analyze such spots. Since the STM image does not provide information about the small lattice vector of the reconstruction supercell, the diffraction simulation produces spots which are not observed in the FFT images. For the sake of clarity, only the multiscattering spots that correspond to the periodicity of the dislocation lines are shown in the simulation of the diffraction pattern.

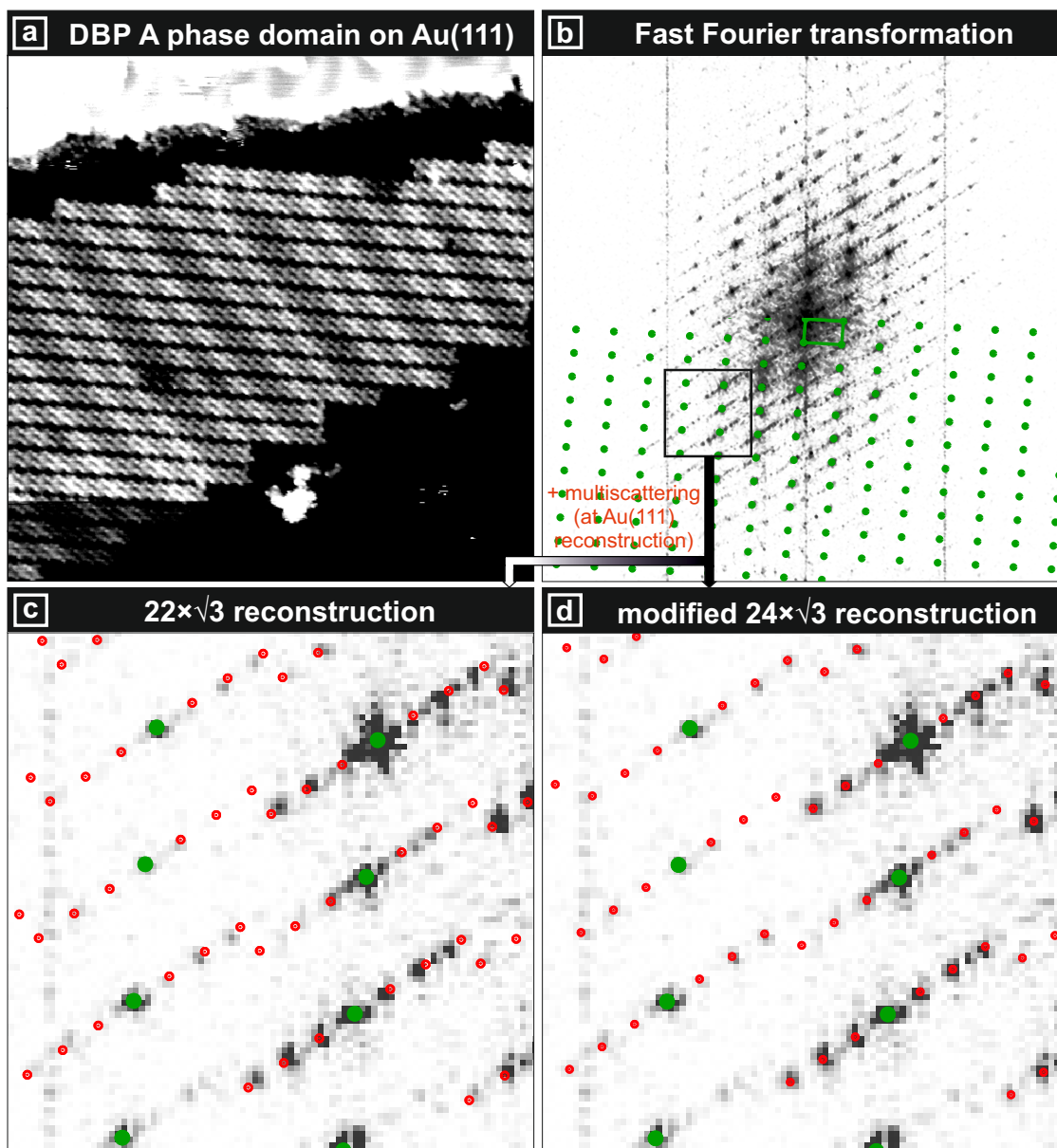


Figure S3: (a) STM image of an *A*-phase domain of DBP on Au(111) (1 V, 50 pA). The dislocation lines of the Au(111) surface reconstruction underneath the molecular domain are clearly visible. The linear grayscale is adjusted for high contrast of the dislocation lines and individual molecules. (b) Contrast-inverted FFT of the STM image in (a) obtained by Gwyddion.¹ Dark areas correspond to high intensities. The simulated diffraction pattern (for details see text) obtained by LEEDLab² is superimposed on the lower half of the image. The reciprocal adsorbate lattice is depicted in green. (c), (d) Close-up view of the region marked by a black square in (b). The simulated multiscattering spots (red) originate from the surface reconstruction with a periodicity of 22 and 24 Au(111) bulk lattice constants in (c) and (d), respectively. Not all multiscattering spots are shown since the STM image does not contain information about the short lattice vector of the Au(111) reconstruction supercell.

Surprisingly, the locations of these spots are not exactly reproduced by the diffraction simulation based on the regular $(22 \times \sqrt{3})$ reconstruction (Figure S3c). While the simulated multiscattering spots (red) are too far apart from the central spots of the reciprocal *A*-phase lattice (green), the direction along which these spots appear is in accordance with the LEED analysis. Therefore, a modification of the periodicity of the Au(111) surface reconstruction has to be taken into account. In the example of Figure S3 the best agreement between the simulation and the FFT spots is achieved when the long lattice vector of the reconstruction supercell is expanded over 24 (rather than 22) Au(111) bulk lattice constants (Figure S3d). Similar analyses of multiple STM images reveal a modification of the Au(111) surface reconstruction toward a $((24 \pm 1) \times \sqrt{3})$ by the presence of DBP *A*-phase domains.

***B* Phase**

DBP domains in the *B*-phase exhibit a higher degree of lateral disorder than *A*-phase domains. Additionally, the adsorption of *B*-phase DBP molecules on Au(111) induces many different modifications of the surface reconstruction, which are not as regular as underneath *A*-phase domains. However, preferred orientations with respect to the Au(111) surface reconstruction are also observed for the *B* domains. The adsorbate lattice vectors enclose $\approx 45^\circ$ with the dislocation lines and the two molecules of the herringbone unit cell are aligned with their long molecular axes parallel and perpendicular to these lines.

Figure S4a shows an STM image of pristine Au(111). The pairs of soliton walls are visible as elongated protrusions. Face-centered cubic (fcc) and hexagonal close-packed (hcp) stacking regions of the $(22 \times \sqrt{3})$ surface reconstruction exhibit widths of 3.9 ± 0.1 nm and 2.7 ± 0.1 nm, respectively.

Two examples of the modified reconstruction underneath *B*-phase domains are depicted in Figure S4b, c. The STM image in Figure S4b shows that the dislocation lines are nearly equally separated by ≈ 3.2 nm with hcp and fcc stacking regions hosting a single row of DBP molecules each. In Figure S4c an STM image is shown where fcc stacking regions exhibit a

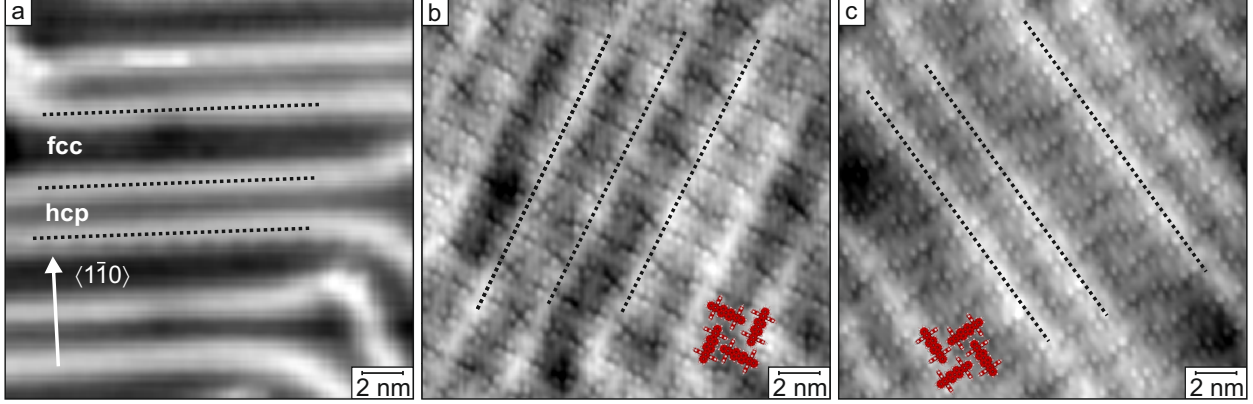


Figure S4: (a) STM image of the pristine Au(111) surface (0.5 V, 100 pA, 20 nm \times 20 nm). The soliton walls of the $(22 \times \sqrt{3})$ reconstruction are visible as elongated protrusions. Face-centered cubic (fcc) and hexagonal close-packed (hcp) stacking regions are indicated. The arrow denotes a crystallographic direction, $\langle 1\bar{1}0 \rangle$. (b), (c) STM images of Au(111) covered with *B*-phase DBP (1 V, 50 pA, 20 nm \times 20 nm). The images show surface regions where the Au(111) reconstruction is differently affected by the presence of adsorption phase *B*. The dashed lines indicate the soliton walls of the modified $(22 \times \sqrt{3})$ surface reconstruction. Ball-and-stick sketches of the DBP molecule have been added as a guide to the eye.

width of 5 nm hosting two rows of DBP molecules.

Analyses of the reconstruction modification by DBP *B*-phase domains from Fourier-transformed STM images were performed analogously to the *A*-phase. The analysis of the FFT spot pattern, corresponding to the STM image in Figure S5a, is exemplarily shown in Figure S5b–d. The spots cannot be reproduced when considering an unmodified $(22 \times \sqrt{3})$ surface reconstruction (Figure S5c). The best agreement is obtained for an expansion of the reconstruction periodicity over 26 Au(111) bulk lattice constants (Figure S5d). This value varies for different STM images, and the contrast of the FFT images is inferior to the images of *A* domains due to the irregularities of the reconstruction underneath *B* domains. Therefore, the analysis of the modification, revealing a $((26 \pm 2) \times \sqrt{3})$ supercell, is accompanied by a rather high error margin. Compared to the *A*-phase, the widths of hcp and fcc regions are altered to a higher extent underneath *B* domains. The hcp stacking regions are tendentially widened.

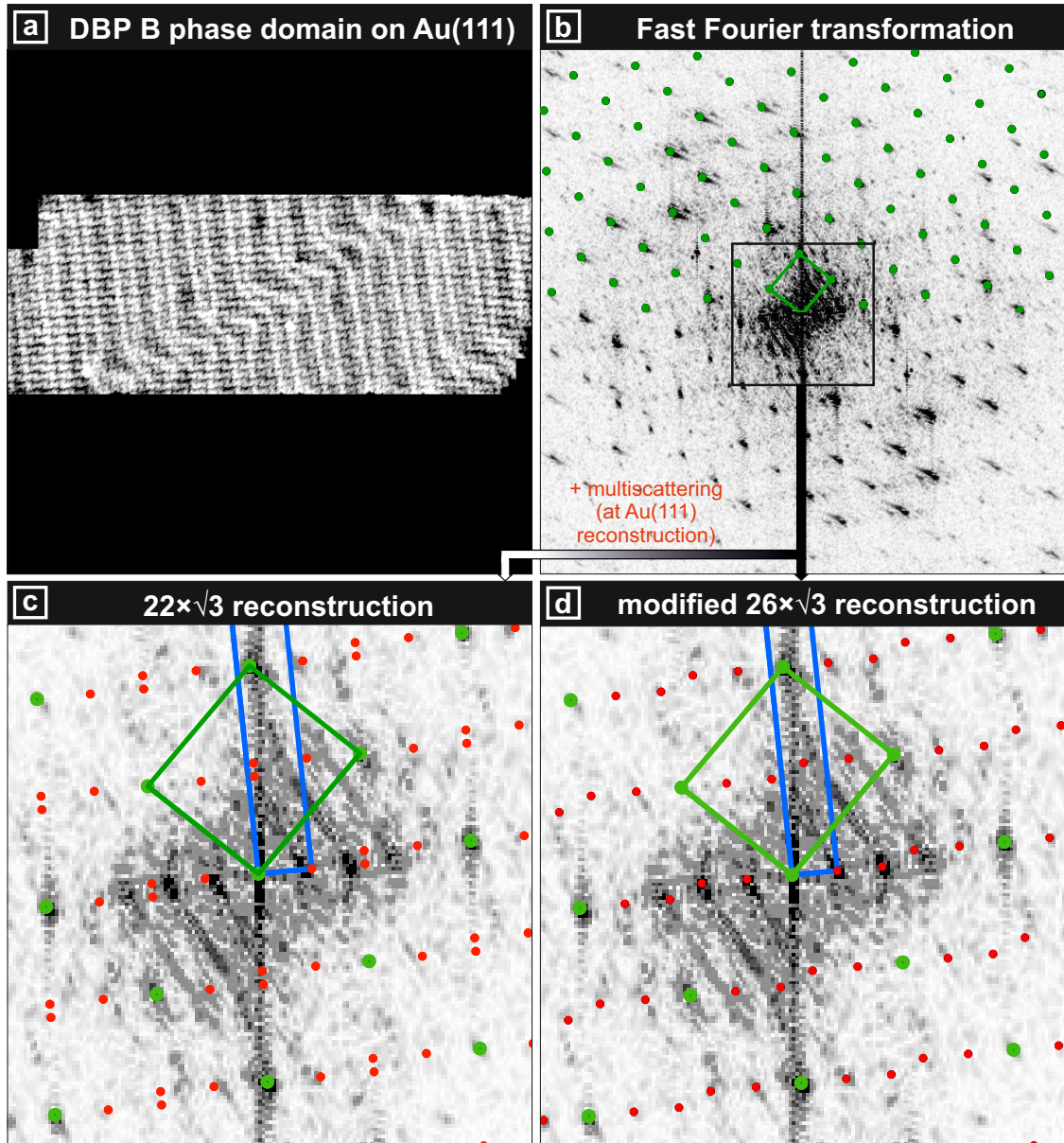


Figure S5: (a) STM image of a *B*-phase domain of DBP on Au(111) (1 V, 30 pA). The dislocation lines of the Au(111) surface reconstruction are clearly visible underneath the molecular island. The image was cut to the size of the *B*-domain and leveled by polynomial corrections. The linear grayscale is adjusted for high contrast of the dislocation lines and individual molecules. (b) Contrast-inverted FFT of the STM image in (a) obtained by Gwyddion.¹ Dark areas correspond to high intensities. The simulation of the diffraction pattern (for details see text) by means of LEEDLab² is superimposed on the upper half of the image. The reciprocal adsorbate lattice is depicted in green. (c), (d) Close-up view of the region marked by a black square in (b). The simulated multiscattering spots (red) originate from the surface reconstruction with a periodicity of 22 and 26 Au(111) bulk lattice constants in (c) and (d), respectively. Not all multiscattering spots are shown since the STM image does not contain information about the short lattice vector of the Au(111) reconstruction supercell. The reciprocal Au(111) reconstruction super cell is superimposed in blue.

Epitaxy of the DBP Adsorption Phases

In the following, the epitaxy relations of the DBP adsorption phases A and B with respect to the Au(111) bulk lattice and the modified surface reconstructions are discussed. The epitaxy matrices are presented in Table S1. The coincidences of phase A in real space are visualized by the structure model in Figure S6.

Table S1: Epitaxy relations of the DBP adsorption phases A and B on Au(111). \mathbf{M}_{bulk} is the epitaxy matrix in relation to the unreconstructed Au(111) surface unit cell, as determined by means of LEED experiments. The numbers in parentheses indicate the uncertainties of the last significant digits. \mathbf{M}_{reco} is the epitaxy matrix in relation to the modified reconstructed Au(111) surface, where $n + 1$ surface atoms occupy the space of n atoms of the Au(111) bulk in the reconstructed direction. The substrate lattice vectors are defined as the vectors which enclose an angle of $\angle \leq 120^\circ$.

Phase	\mathbf{M}_{bulk}	n	\mathbf{M}_{reco}
A	$\begin{pmatrix} 4.87(1) & 3.12(1) \\ -0.85(2) & 6.85(1) \end{pmatrix}$	24	$\begin{pmatrix} 5.01 & 3.12 \\ -1.02 & 6.85 \end{pmatrix}$
B	$\begin{pmatrix} 8.14(4) & 5.96(5) \\ -2.51(4) & 6.72(6) \end{pmatrix}$	26	$\begin{pmatrix} 8.33 & 5.96 \\ -2.74 & 6.72 \end{pmatrix}$

As already pointed out in the manuscript, the epitaxy matrix \mathbf{M}_{bulk} of structure A indicates an on-line coincidence with the unreconstructed Au(111) surface, as the sum of the matrix elements of each row is integer within the experimental accuracy.⁴ Coincidences in reciprocal space occur for the $(h_a = 8, k_a = 6)$ lattice points of the adsorbate and the $(h_s = 1, k_s = 1)$ lattice points of the substrate. In this case, all adsorbate lattice points are located on the equidistant [11] lines of the Au(111) bulk lattice, as indicated by blue lines in Figure S6.

The epitaxy matrices \mathbf{M}_{reco} , which refer to the modified surface reconstructions, are given under the assumption that $n + 1$ surface atoms occupy the space of n atoms of the Au(111) bulk in the reconstructed direction. Consequently, an idealized surface reconstruction underneath A -phase domains is assumed, where 25 atoms are equidistantly distributed over 24 bulk lattice constants. Furthermore, a primitive unit cell of the reconstructed surface lattice

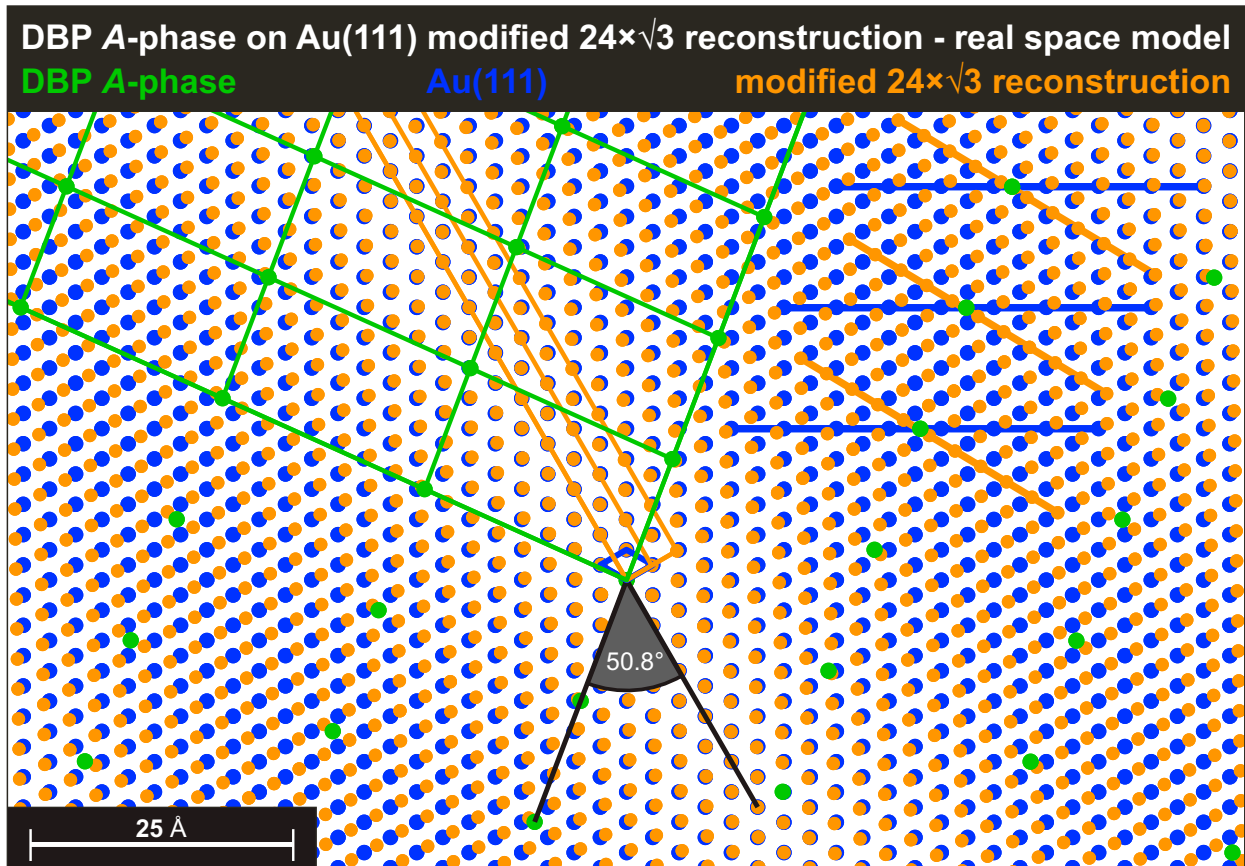


Figure S6: Real space models of the *A*-phase lattice (green), together with the Au(111) bulk lattice (blue) and the modified ($24 \times \sqrt{3}$) reconstruction supercells (orange). The orange (blue) lines indicate the possible on-line coincidences with the reconstructed (unreconstructed) substrate lattice. All adsorbate lattice points are located on these lines.

is defined, where the lattice vectors enclose an angle of $\angle \leq 120^\circ$.

For structure *A* this matrix indicates a point-on-line epitaxy with respect to the modified reconstruction, as the first column values are close to integers. Coincidences in reciprocal space occur for the $(h_a = 5, k_a = -1)$ lattice points of the adsorbate and the $(h_s = 1, k_s = 0)$ lattice points of the substrate. In real space all adsorbate lattice points are located on [10] lines of the $(24 \times \sqrt{3})$ Au(111) reconstruction, which represent primitive directions of the surface lattice, as indicated by orange lines in Figure S6.

Neither the epitaxy matrix \mathbf{M}_{bulk} nor the matrix \mathbf{M}_{reco} of structure *B* reveal any particular epitaxy type with respect to the unreconstructed surface and the $(26 \times \sqrt{3})$ Au(111) reconstruction. This observation is not surprising since the epitaxial relations of the *B*-phase are estimations for an average adsorbate–substrate relationship. The *B*-phase domains as well as the reconstructed Au(111) surface underneath are rather flexible lattices, which might adjust to each other. Such local relaxations were reported to cause a total energy gain for other monolayer films of aromatic molecules, such as hexa-*peri*-hexabenzocoronene on graphite.³ Similar mechanisms are also conceivable for the relaxations of both, the *B*-phase lattice and the Au(111) surface. This might cause distortions of the long-range order and fluctuations of the lateral molecular density, which are observed in our STM experiments. Most likely, the molecular adsorption sites within the *B*-phase domains are determined by these local relaxations rather than by a rigid epitaxial relation in the context of the classical epitaxy definition.

DBP Orbital Electronic Structure on Au(111)

In order to explore the orbital electronic structure of *A*-phase and *B*-phase DBP on Au(111) spectroscopy of the differential conductance (dI/dV) was performed on individual molecules at 77 K using a standard lock-in technique (modulation voltage: 10 mV_{rms}, modulation frequency: 850 Hz).

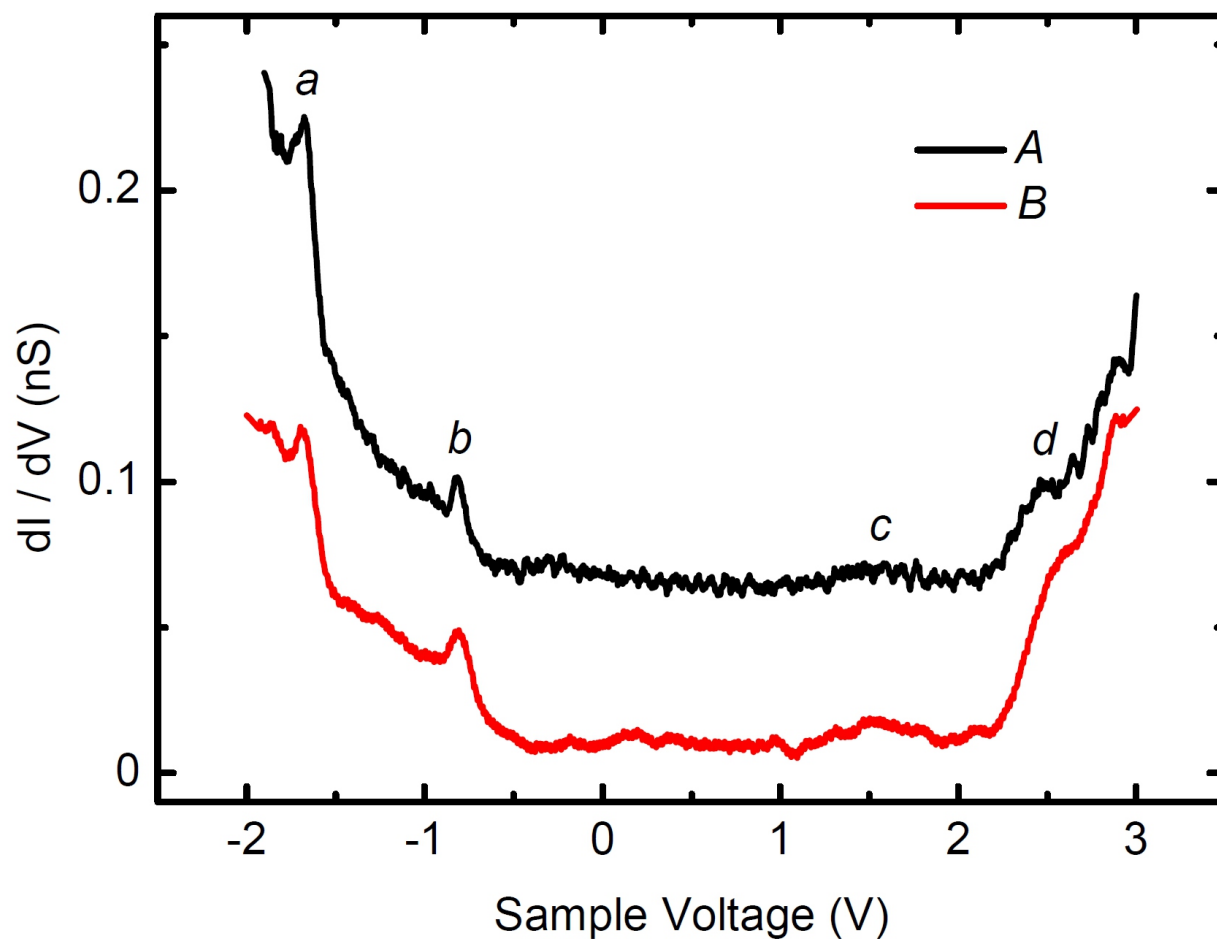


Figure S7: Constant-height spectra of the differential conductance (dI/dV) acquired atop *A*-phase (top) and *B*-phase (bottom) DBP on Au(111). The spectra represent data averaged over several positions of the individual molecule. The feedback loop had been disabled at 3 V and 100 pA prior to data acquisition. The spectrum of *A*-phase DBP was offset by 0.05 nS.

Figure S7 shows dI/dV spectra acquired atop *A*-phase (upper data set) and *B*-phase (lower data set) DBP molecules. The spectra represent data that were spatially averaged over different positions of the individual molecule. Occupied molecular orbitals appear as peaks at ≈ -1.68 V (*a*) and ≈ -0.81 V (*b*) for both adsorption phases. At positive bias voltages unoccupied orbitals are visible as a weak and broad feature at ≈ 1.55 V (*c*) for *A*-phase and *B*-phase DBP. Additionally, a shoulder (*d*) occurs at ≈ 2.50 V for *A*-phase DBP and at ≈ 2.60 V for *B*-phase DBP. The Shockley surface state of Au(111) is not visible in the spectra, which contrasts results obtained for PTCDA on Au(111).⁵ We can tentatively assign features *c* and *d* to the spectroscopic signatures of the lowest unoccupied molecular orbital (LUMO) and to the next-to-lowest unoccupied molecular orbital (LUMO+1). For the free DBP molecule charge density isosurfaces were calculated.⁶ The calculated spatial distribution of the LUMO is comparable with our findings in maps of dI/dV acquired at the bias voltage for feature *c* (not shown). In addition, the calculated LUMO+1 energy is ≈ 1 eV higher than the LUMO energy,⁶ which matches the energy difference between *c* and *d* reasonably well. The calculated energy gap between the highest occupied molecular orbital (HOMO) and the LUMO is ≈ 2.30 eV. This energy corresponds well to the voltage gap of ≈ 2.36 V between the feature *b* and the LUMO feature *c*. Moreover, the calculated next-to-highest occupied molecular orbital (HOMO-1) energy is ≈ 0.86 eV below the HOMO, which is in accordance with the bias voltage distance of 0.87 V between features *a* and *b*.⁶ The features *b* and *a* are therefore attributed to the spectroscopic signatures of the HOMO and the HOMO-1, respectively.

The similarity of the spectra indicates akin interface properties of the different adsorption phases. In particular, possibly different charge transfer between Au(111) and *A*-phase / *B*-phase DPB is difficult to infer from the spectroscopic data.

References

- (1) Necas, D.; Klapetek, P. Gwyddion: an open-source software for SPM data analysis. *Centr. Eur. J. Phys.* **2012**, *10*, 181–188.
- (2) LEEDLab and LEEDCal are commercially available at <http://www.scientaomicron.com/en/products/350/1155> and <http://www.scientaomicron.com/en/products/350/1154>, respectively.
- (3) Meissner, M.; Sojka, F.; Matthes, L.; Bechstedt, F.; Feng, X.; Müllen, K.; Mannsfeld, S. C. B.; Forker, R.; Fritz, T. Flexible 2D Crystals of Polycyclic Aromatics Stabilized by Static Distortion Waves. *ACS Nano* **2016**, *10*, 6474–6483.
- (4) Forker, R.; Meissner, M.; Fritz, T. Classification of epitaxy in reciprocal and real space: rigid versus flexible lattices. *Soft Matter* **2017**, *13*, 1748–1758.
- (5) Kröger, J.; Jensen, H.; Berndt, R.; Rurali, R.; Lorente, N. Molecular orbital shift of perylenetetracarboxylic-dianhydride on gold. *Chem. Phys. Lett.* **2007**, *438*, 249–253.
- (6) Kirchhübel, T.; Gruenewald, M.; Sojka, F.; Kera, S.; Bussolotti, F.; Ueba, T.; Ueno, N.; Rouillé, G.; Forker, R.; Fritz, T. Self-Assembly of Tetraphenyldibenzoperiflanthene (DBP) Films on Ag(111) in the Monolayer Regime. *Langmuir* **2016**, *32*, 1981–1987.